Composites Part B 215 (2021) 108746

Contents lists available at ScienceDirect

Composites Part B

journal homepage: www.elsevier.com/locate/compositesb

Process optimization, microstructure characterization and thermal properties of mesophase pitch-based carbon fiber reinforced aluminum matrix composites fabricated by vacuum hot pressing

Chengnan Zhu [a], Yishi Su [a,**], Xiaoshu Wang [a], Haicheng Sun [b], Qiubao Ouyang [a,*], Di Zhang [a]

[a] State Key Laboratory of Metal Matrix Composites, School of Materials Science and Engineering, Shanghai Jiao Tong University, 800 Dongchuan Road, Shanghai, 200240, China
[b] Tiance Technology Co. Ltd, Xi'an National Civil Aerospace Industrial Base, Shanxi, 710100, China

ARTICLE INFO

Keywords:
Carbon fiber
Metal-matrix composites (MMCs)
Sintering
Thermal properties
Microstructures

ABSTRACT

Continuous mesophase pitch-based carbon fiber (MPCF) reinforced aluminum (Al) matrix composites were fabricated by vacuum hot pressing to meet the requirements of good thermal conductivity (TC), low coefficient of thermal expansion (CTE) and resistance to deformation for thermal management materials. The effect of process parameters on the microstructures and TC of 40 vol % MPCF/Al composites and the influence of MPCF volume fraction on the thermal-mechanical properties of MPCF/Al composites were studied. The results reveal that the composites with 20–50 vol % MPCF fabricated at 650 °C/45 MPa/60 min have longitudinal TC of 230.3–288.3 W/(m·K), over 90% of the predictions by rule of mixture, longitudinal CTE of 2.28−-0.22 ppm/K and elastic modulus of 147.5–324 GPa. The interface is mainly composed of an amorphous interface layer of 2–5 nm and a very small amount of carbide crystals. Furthermore, these composites have moderate TC, lower CTE and higher specific modulus compared with other Al matrix composites and Al alloys, which indicates they are expected to become unidirectional thermal management materials with integrated structure and function.

1. Introduction

In the fields of power electronics and aerospace, with the continuous development of electronic components in terms of power and miniaturization, equipment will generate more heat [1–3]. In order to improve the performance, reliability and service life of the equipment, it is necessary to develop thermal management materials with good thermal conductivity (TC), low coefficient of thermal expansion (CTE) and resistance to deformation [4,5]. Besides, lightweight is also their development trend [6]. Composites have long been considered as promising potential thermal management materials because of their tunable thermal properties [7]. Among them, metal matrix composites are the most popular, because they not only have good TC, but also have good mechanical properties, high-temperature resistance and oxidation resistance [3,8]. Aluminum (Al) and copper (Cu) are often used as the matrix due to their relative universality and good stability [8,9]. However, as lightweight thermal management materials, Al matrix composites have more advantages because the density of Al is much lower than that of Cu [10–12]. Carbon fibers (CF) is often used as the reinforcement for aluminum matrix composites due to its high specific modulus, high specific strength and low CTE [13,14]. It is normally divided into polyacrylonitrile (PAN)-based CF, Rayon-based CF and pitch-based CF according to the different precursors [15–17]. PAN-based CF is the most widely used, occupying 96% of the carbon fiber market. It has the characteristics of high strength and low TC. Rayon-based carbon fiber has lower modulus, strength and TC than PAN-based CF and pitch-based CF, so its application is limited. Pitch-based CF is commonly classified into isotropic pitch-based carbon fiber (IPCF) and mesophase pitch-based carbon fiber (MPCF) [15]. Among them, MPCF has received extensive attention in recent years. Because it not only has ultra-high modulus (>600 GPa), but also has anisotropic thermal properties, a high TC (up to 1100 W/(m·K)) and a low CTE (−1.5 to −1 ppm/K) in the longitudinal direction (fiber axis), and a low TC (2–10 W/(m·K)) and a medium CTE (10–15 ppm/K) in the transverse direction (fiber radial) [15,18,19], which is beneficial to improve the resistance to deformation, TC and reduce the CTE of Al

* Corresponding author.
** Corresponding author.
E-mail addresses: suyishi@sjtu.edu.cn (Y. Su), oyqb@sjtu.edu.cn (Q. Ouyang).

https://doi.org/10.1016/j.compositesb.2021.108746
Received 1 November 2020; Received in revised form 20 February 2021; Accepted 23 February 2021
Available online 27 February 2021

matrix composites in a certain direction. Also, its graphitization degree is relatively high [15], which is beneficial to reduce the interfacial reaction between CF and Al.

In the past two decades, there have been many studies on the mechanical properties of CF/Al composites [14,20–23], but there are relatively few studies on the thermal properties of MPCF/Al composites, mainly as summarized in Table 1, it can be seen that these studies are mainly focused on the discontinuous MPCF/Al composites. However, few studies have been reported on the continuous MPCF/Al composites. It is really worth studying the thermal properties of continuous MPCF/Al composites. First, the dispersion of continuous MPCFs is more difficult than that of discontinuous MPCFs. When continuous MPCF/Al composites are fabricated at relatively low temperatures (below the melting point of Al), it is relatively difficult for Al to enter the MPCF bundles. Second, this ultra-high modulus CF has extremely high brittleness, so it is easy to break during the preparation of composites [24]. Discontinuous MPCF/Al composites generally do not need to consider the effect of fiber breakage, while continuous MPCF/Al composites need to consider the effect of fiber breakage to obtain excellent properties. In addition, for the aerospace field, such as antenna boom for the space telescope [6,25], it will undergo about 175,000 thermal cycles from +125 °C to −125 °C when operating in outer space. Therefore, it is required to have high dimensional stability to maintain internal dimensional tolerance of ±0.15 mm along the entire length in the presence of dynamic and thermal disturbances [26]. The material with high specific modulus and low CTE can provide the necessary characteristics to produce dimensionally stable structures. Continuous MPCF/Al composites can more easily meet these requirements.

Vacuum pressure infiltration [27,28] and squeeze casting [29,30] are the main methods for fabricating continuous MPCF/Al composites, because these methods allow the easy densification of Al matrix composites with high volume fractions of reinforcement, but they are not suitable for the composites with low volume fractions of reinforcement. Moreover, the process of these methods is relatively complicated, and they need to prepare MPCF preforms. The composite samples must be obtained through secondary processing. As far as we know, there are few studies on the fabrication of continuous MPCF/Al composites by vacuum hot pressing (VHP), but this method is commonly used to fabricate the composites with low and medium volume fractions of reinforcement, and its process is relatively simple. The composite samples can be obtained through one-time molding. Besides, the fabrication temperature of this method is relatively low, so the interfacial reaction of carbon material/Al composites is relatively weak, and it is relatively easy to control the interfacial reaction by adjusting the process parameters [9,31,32].

In this work, 40 vol % MPCF/Al composites were fabricated by VHP. The effect of process parameters (sintering temperature, sintering pressure and sintering time) on microstructures and TC (longitudinal/transverse) of the composites was investigated. The process parameters were optimized to obtain MPCF/Al composites with high longitudinal TC. Afterward, optimized process parameters were used to fabricate MPCF/Al composites with 20–50 vol % MPCF, and their microstructures, interfaces and thermal-mechanical properties were studied. Furthermore, the thermal-mechanical properties of these composites were compared with those of Al matrix composites and Al alloys that may be used as thermal management materials in the references. The reasons why these composites have good TC, low CTE and high specific modulus were also discussed.

2. Experimental

2.1. Raw materials and composites fabrication

In this work, pure Al powders (~10 μm in diameter, 99.5% in purity, Henan Yuanyang Powder Technology Co. ltd) were selected as matrix and 2K MPCFs (TC-HM-70, TianCe Technology Co. ltd) were selected as reinforcements. Their morphologies are shown in Fig. 1(a) and (b), respectively. Table 2 presents the basic properties of MPCF.

Fig. 1(c) shows the schematic diagram of the fabrication process of MPCF/Al composites. The specific processes are listed as follows: (1) 5 g MPCFs with a length of 40 mm were immersed in 100 ml acetone for 12 h to remove the sizing resin, then washed with deionized water and dried at 90 °C for 6 h in a vacuum drying oven. (2) The dried MPCFs were dispersed, and then 0.057 g MPCFs were mixed with 0.168 g Al powders by a roller ball mill at a low speed of 20 rpm for 2 h. In order to adjust the MPCF volume fraction in the composites, 0.057 g MPCFs were mixed with 0.288 g, 0.108 g and 0.072 g Al powders, respectively. (3) The prepared MPCFs mixed with Al powders were carefully filled into the clean graphite mold (40 × 20 mm^2) by stacking method, and then heated to the desired temperature (620, 640, 650 and 660 °C) in a high vacuum condition (below 5 × 10^{-2} Pa) and kept for some time (40, 60, 80 and 100 min), while a uniaxial pressure (35, 45 and 55 MPa) was applied. After the sintering process was completed, the uniaxial pressure was removed and the furnace was cooled to room temperature. Finally, rectangular samples (40 × 20 × 2 mm^3) were taken out of the furnace, and the test samples were taken from the middle of the rectangular samples.

2.2. Experimental method and characterization

The samples used to test the CTE of the composites were treated by thermal cycling (0, 50 and 100 cycles). During the thermal cycling, the samples were held at 120 °C for 35 min in 101A-1 furnace (Shanghai Laboratory Instrument Works Co., Ltd., China), and then held in liquid nitrogen (−196 °C) for 25 min. The temperature accuracy value of 101A-1 furnace was ±5 °C.

Phase compositions of MPCF and MPCF/Al composites were identified by X-ray diffraction (XRD, Rigaku and CN2301, Japan) with Cu Kα radiation. Microstructures of MPCF/Al composites were characterized by optical microscopy (OM, ZEISS Axio Scope.A1, Germany) and scan-

Table 1
Thermal properties of MPCF/Al composites.

Material	Type of MPCF	TC of MPCF (W/(m·k))	V_f (%)	TC (W/(m·k))	CTE (ppm/K)	Fabrication method	References
MPCF/Al	Discontinuous	900	_	186.3	_	Vacuum pressure infiltration	[53]
MPCF/Al	Discontinuous	900	40	208	_	Vacuum pressure infiltration	[54]
MPCF/Al	Discontinuous	320	30	_	15.5 (50-150 °C)	Hot pressing	[9]
MPCF/Al	Discontinuous	900	40	221	9.4 (100-300 °C)	Vacuum pressure infiltration	[39]
MPCF/Al-Cu	Continuous	800	30	273.2	_	Low pressure infiltration	[27]
MPCF/Al	Discontinuous	900	50	238	_	Spark plasma sintering	[34]
MPCF/Al-Si	Continuous	800	30	182	_	Low pressure infiltration	[28]
MPCF/Al-Si	Discontinuous	1200	40	323	_	Hot extrusion	[55]
MPCF/Al(A1070)	Discontinuous	800	10	245.8	_	Low pressure casting	[56]
MPCF/Al(A336)	Discontinuous	800	10	113.5	_	Low pressure infiltration	[57]
MPCF/6063Al	Continuous	600	70	407	−1–1 (50-500 °C)	Squeeze casting method	[29]
MPCF/Al-3Mg	Discontinuous	500–600	2.5	134.9	_	Extrusion	[58]
MPCF/Al-Si	Discontinuous	600	50	258	7 (100-180 °C)	Semi-liquid process	[10,59]

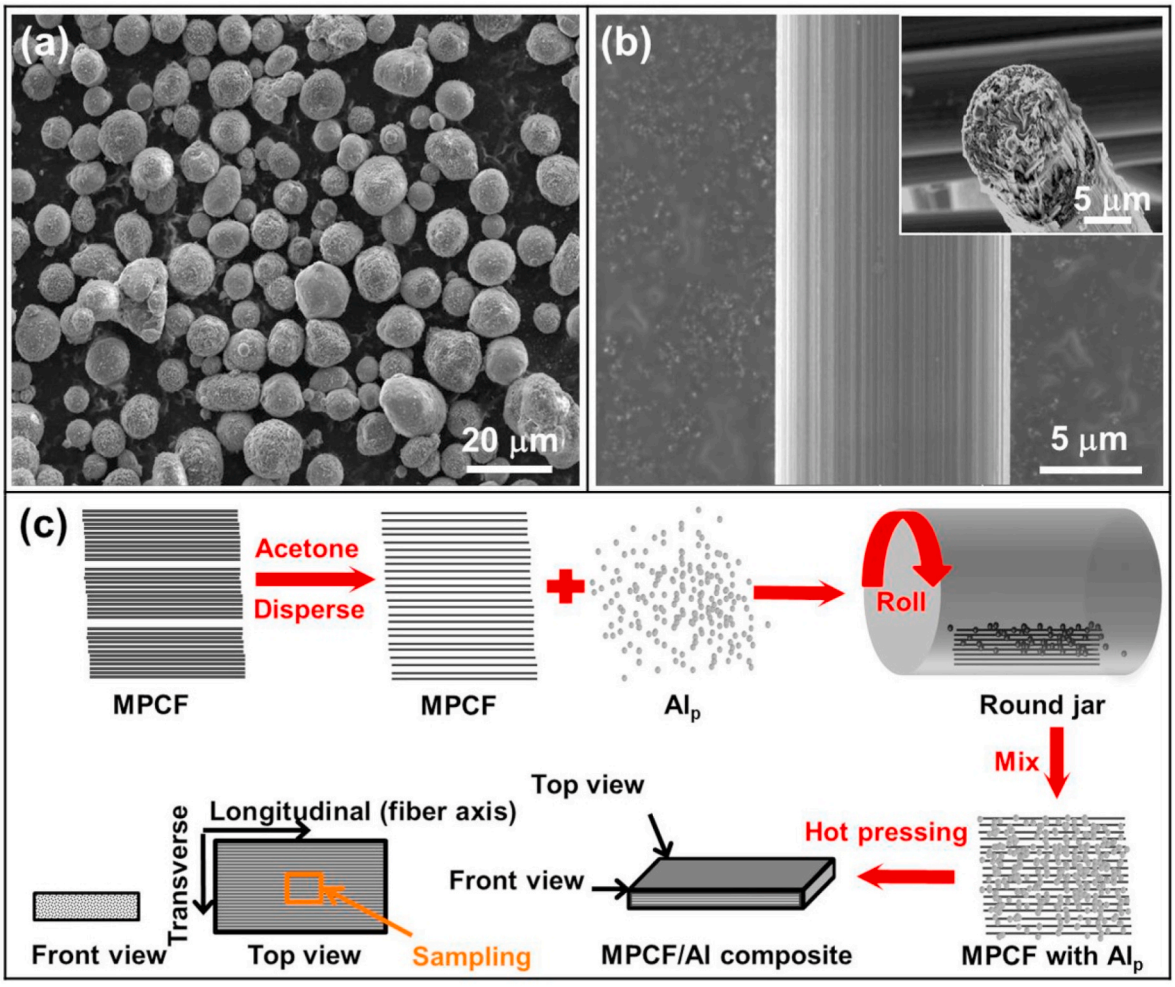

Fig. 1. Morphologies of (a) Al powders, (b) MPCF; (c) Schematic diagram of the preparation process of MPCF/Al composites.

Table 2
Basic properties of MPCF.

Diameter (μm)	ρ_f (g/cm^3)	UTS (MPa)	E_f (GPa)	C_f (J/g/K)	TC (W/(m·K)) L T		CTE (ppm/K) L T	
13	2.12	2200	750	0.712	396.4	2.4 [24]	−1.5	10-15 [59]

L: Longitudinal; T: Transverse

ning electron microscopy (SEM, TESCAN MIRA3, Czech Republic). The element distribution of the composites was determined by energy dispersive spectroscopy (EDS). The interfacial microstructure of the composites was characterized by a field emission transmission electron microscope (FE-TEM, Talos F200X G2, China). The TEM sample was fabricated by using a focused ion beam (FIB, GAIA3, Czech Republic) apparatus. The TC values of the composite samples were calculated from the product of the density, specific heat capacity and thermal diffusivity. The densities of the samples were measured by the Archimedes method. The specific heat capacities of the samples at room temperature were obtained by the following expression (Eq. (1)) [29]:

$$C_c = \frac{V_f \rho_f C_f + (1 - V_f)\rho_m C_m}{\rho_c} \quad (1)$$

In Eq. (1) V, ρ and C are volume fraction, density and specific heat capacity, and the subscripts *c, m,* and *f* refer to the composite, matrix and reinforcement, respectively. The thermal diffusivities of the samples (10 × 10 × 2 mm^3) at room temperature were tested using a laserflash thermal conductivity (NETZSCH LFA 447, Germany). The thermal expansion behaviors of the samples (25 × 6 × 2 mm^3) were examined by thermal dilatometer (NETZSCH DIL 402 Expedis, Germany). The tested temperature ranged from 25 to 250 °C with a heating rate of 5 °C/min in an argon atmosphere. According to ASTM D3552-17, tensile specimens of the composites with the gauge length of 15 mm, gauge width of 4 mm and thickness of 2 mm were machined parallel to the fiber's orientation. Three uniaxial tensile tests for each set of specimens were performed using a universal testing machine (Zwick/Roell Z020, 20 KN, Japan) under a uniaxial tensile loading at 0.5 mm/min.

3. Results and discussion

3.1. Effect of process parameters on microstructures and thermal conductivity of MPCF/Al composites

3.1.1. Effect of sintering temperature

Fig. 2 shows the appearances, metallographic structures and fracture surfaces of 40 vol % MPCF/Al composites sintered at different temperatures (620, 640, 650, and 660 °C) for 100 min under pressure of 55

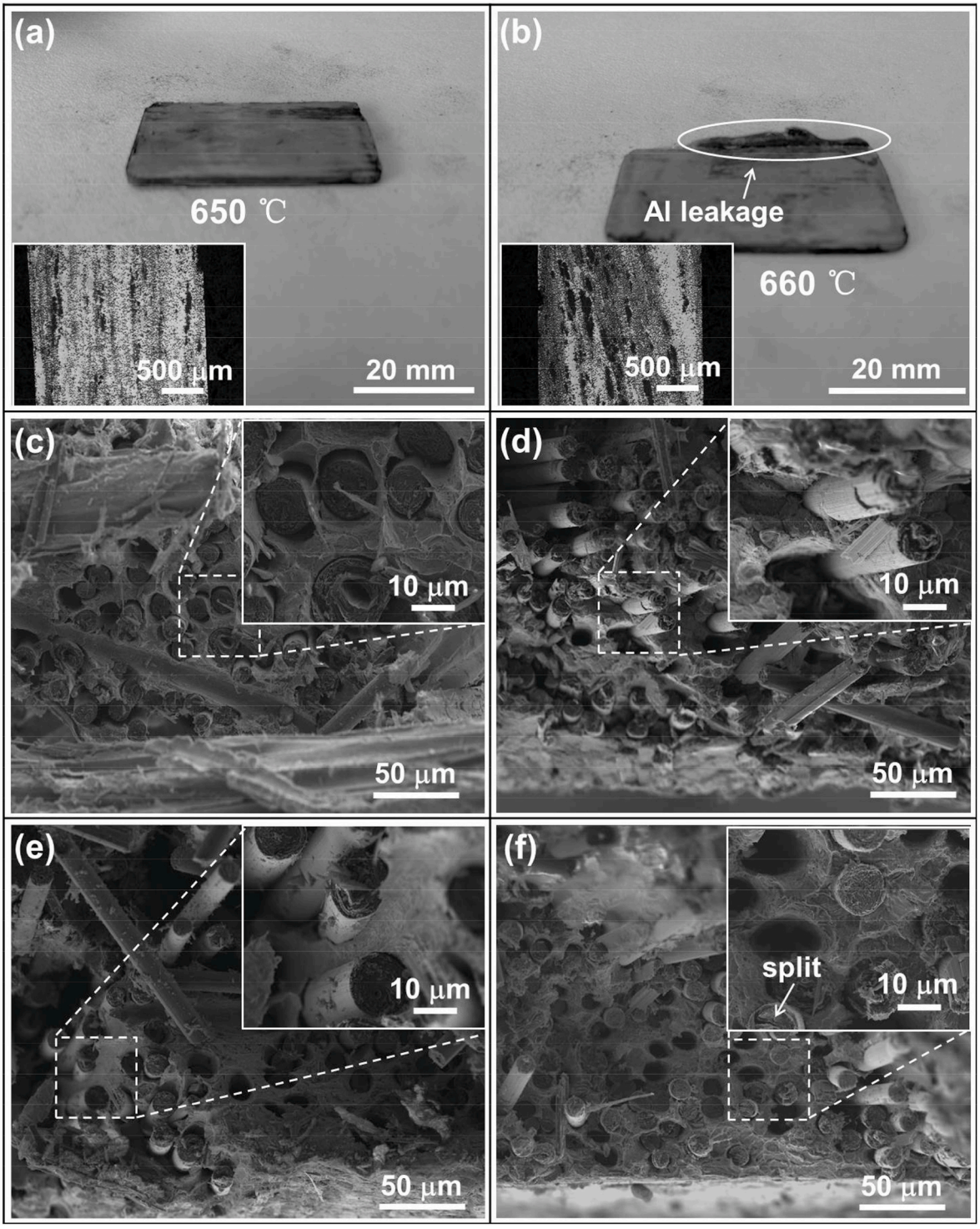

Fig. 2. Appearances, metallographic structures and fracture surfaces of 40 vol % MPCF/Al composites sintered at different temperatures for 100 min under pressure of 55 MPa: (a) appearance and metallographic structure, 650 °C; (b) appearance and metallographic structure, 660 °C; (c) fracture surface, 620 °C; (d) fracture surface, 640 °C; (e) fracture surface, 650 °C; (f) fracture surface, 660 °C.

MPa. As shown in Fig. 2(a), the appearance of the composite sample sintered at 650 °C is complete. From the inset of the transverse metallographic structure on the bottom left of the figure, it can be seen that most of the MPCFs are surrounded by Al, and a small amount of MPCFs are agglomerated in the local area. While in Fig. 2(b), there is Al leakage at the edge of the composite sample sintered at 660 °C, and it can be seen that the distribution of MPCFs in the composite is uneven and the phenomenon of fiber aggregation in the composite becomes serious according to the inset of the transverse metallographic structure on the bottom left of the figure. This is caused by the fabrication temperature close to the melting point of Al. As shown in Fig. 2(c), while the sintering temperature is 620 °C, it can be clearly seen that the MPCF and Al are completely debonded, which means that the interfacial bonding between them is very weak. While the sintering temperature increases to 640 °C, the phenomenon of complete debonding is significantly reduced according to Fig. 2(d). For the composite sintered at 650 °C, the MPCF

and Al are partially debonded, and Al adheres to the MPCF surface in local areas according to Fig. 2(e), which indicates that the interfacial bonding between MPCF and Al has been improved. If the sintering temperature continues to increase to 660 °C, the bonding between MPCF and Al is tight, and splitting of MPCF can even be observed in local areas according to Fig. 2(f), indicating that a strong interfacial bonding has been developed in the composite.

Fig. 3 shows the relative density, longitudinal and transverse TC of the composites sintered from 620 to 660 °C. As shown in Fig. 3(a), when the sintering temperature increases from 620 to 650 °C, the relative density of the composites increases from 94.2% to 97.2%, because the fluidity of Al increases with the increase of temperature, making it easier to enter the gap between MPCFs, and the interfacial bonding between MPCF and Al becomes better. However, the relative density of the composites decreases to 96.7% when the sintering temperature increases to 660 °C, which may be due to the Al leakage. As shown in Fig. 3 (b) and (c), it can be seen that the sintering temperature has an important influence on longitudinal and transverse TC of the composites. When the sintering temperature increases from 620 to 650 °C, the longitudinal TC and transverse TC of the composites increases from 186.0 to 234.5 W/(m·K) and 31.0–39.6 W/(m·K), respectively, but when the sintering temperature increase to 660 °C, the longitudinal TC and transverse TC decreases to 218.1 and 35.4 W/(m·K), respectively. The reason for this change can be explained in this way. Generally, the higher the sintering temperature, the better the interfacial bonding, and the better the TC, but when the sintering temperature is close to 660 °C, the fluidity of Al increases, and Al leakage occurs in the composite. On the one hand, the MPCF volume fraction in the composite becomes higher, which is beneficial to improve the longitudinal TC and reduce the transverse TC of the composites. On the other hand, it is easy to cause fiber aggregation (see from Fig. 2(b)) and increase the pores in the composite [33,34]. This is not conducive to improving the longitudinal and transverse TC of the composites. Therefore, the decrease in longitudinal TC of the composite sintered at 660 °C is mainly due to the increase of defects, and the decrease in transverse TC may be due to the increase of MPCF volume fraction and defects in the composite. According to the above analysis, the composite sintered at 650 °C can obtain relatively high longitudinal and transverse TC. Therefore, 650 °C is chosen as the optimized sintering temperature of MPCF/Al composites to vary the pressure and time for obtaining higher TC.

3.1.2. Effect of sintering pressure

Fig. 4 shows the microstructures of 40 vol % MPCF/Al composites sintered at 650 °C for 100 min under different pressures (35, 45 and 55 MPa). As shown in Fig. 4(a) and (b), when the sintering pressure is 35 MPa, it can be seen that the MPCFs in the local area of the composite are agglomerated seriously, but they are relatively intact and parallel to each other. When the sintering pressure is 45 MPa, the phenomenon of fiber agglomeration is significantly reduced. Most of the relatively intact and parallel MPCFs are surrounded by Al according to Fig. 4(c) and (d), which is beneficial to the heat conduction of the composite. However, when the sintering pressure increases to 55 MPa, although most of the MPCFs are relatively uniformly dispersed in the composite, it can be seen that the orientation of some fibers (marked with white circles) has changed significantly according to Fig. 4(e) and (f), which shows that the intactness of some fibers is damaged and their arrangement in the composite changes.

Fig. 5 shows the relative density, longitudinal and transverse TC of the composites sintered under pressure from 35 to 55 MPa. As shown in Fig. 5(a), the relative density of the composites increases from 94.8% to 97.2% as the pressure increases. It indicates an improvement in consolidation and a reduction in defects in the composite, which is consistent with the results of microstructures of the composites as shown in Fig. 4. As shown in Fig. 5(b) and (c), the longitudinal TC of the composites does not always increase with the increase of the sintering pressure. It first increases from 245.7 to 258.1 W/(m·K), and then when the sintering pressure is 55 MPa, it will decrease by 23.6 W/(m·K). While the transverse TC of the composites increases with the increase of the sintering pressure. It increases from 13.6 to 39.6 W/(m·K), and it has been greatly improved when the sintering pressure is 55 MPa. These changes are related to the relative density of the composites, the intactness and arrangement of MPCFs in the composites. As the sintering pressure increases, the density of the composites increases, which is conducive to improving longitudinal and transverse TC of the composites, while the intactness of MPCFs is damaged and the arrangement of MPCFs in the composites changes, which are unfavorable for the composites to obtain high longitudinal TC. Therefore, in order to ensure that the composite has a high longitudinal TC, 45 MPa is selected as the appropriate pressure.

3.1.3. Effect of sintering time

It is well known that when the 40 vol % MPCF/Al composites are sintered at 650 °C under pressure of 45 MPa, there is a tendency of the generation of Al_4C_3 in the interface, because the standard free energy of Al_4C_3 formation reaction is negative at fabrication temperature (650 °C) [27]. Fig. 6 show the XRD patterns of the composites sintered for different time (40, 60, 80 and 100 min) and MPCFs. As shown in Fig. 6 (a), when the scanning speed is 4°/min in the range of 10–90°, it can be seen that there are two phases in the MPCFs. One is the C70 phase (JCPDS number: 50-1364) with a tetragonal structure, and the peaks at $2\theta = 13.289°$ and 19.085° correspond to its (002) and (201) planes. The other is graphite phase (JCPDS number: 41-1487), and the peaks at $2\theta = 26.381°$ and 54.542° correspond to (002) and (004) planes. In addition, the peaks at $2\theta = 38.472°$, 44.738°, 65.133°, 78.227° and 82.435° corresponded to (111), (200), (220), (311) and (222) planes are observed for the Al phase (JCPDS Number: 04-0787) in the composites, but the Al_4C_3 phase cannot be observed, probably because either no Al_4C_3 is formed at all, or the amount of Al_4C_3 formed is too low relative to the amount of C70, graphite and Al, which cannot be detected at such scanning speed. To verify the presence of the reaction product Al_4C_3, the composites are further examined by XRD at a much lower scanning speed of 0.25°/min in the range of 31–35°, in which the characteristic peaks of Al_4C_3 are included. The corresponding XRD patterns are shown in Fig. 6(b). For the composites sintered for 80 and 100 min, it can be clearly seen the diffractions at the 2θ angles of 31.112°, 31.739°, and 32.232° correspond to the (101), (012) and (009) planes of Al_4C_3,

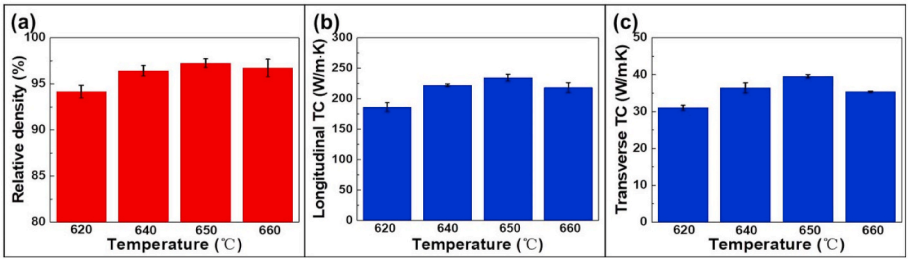

Fig. 3. Effect of sintering temperature on (a) relative density; (b) longitudinal TC; (c) transverse TC of the composites.

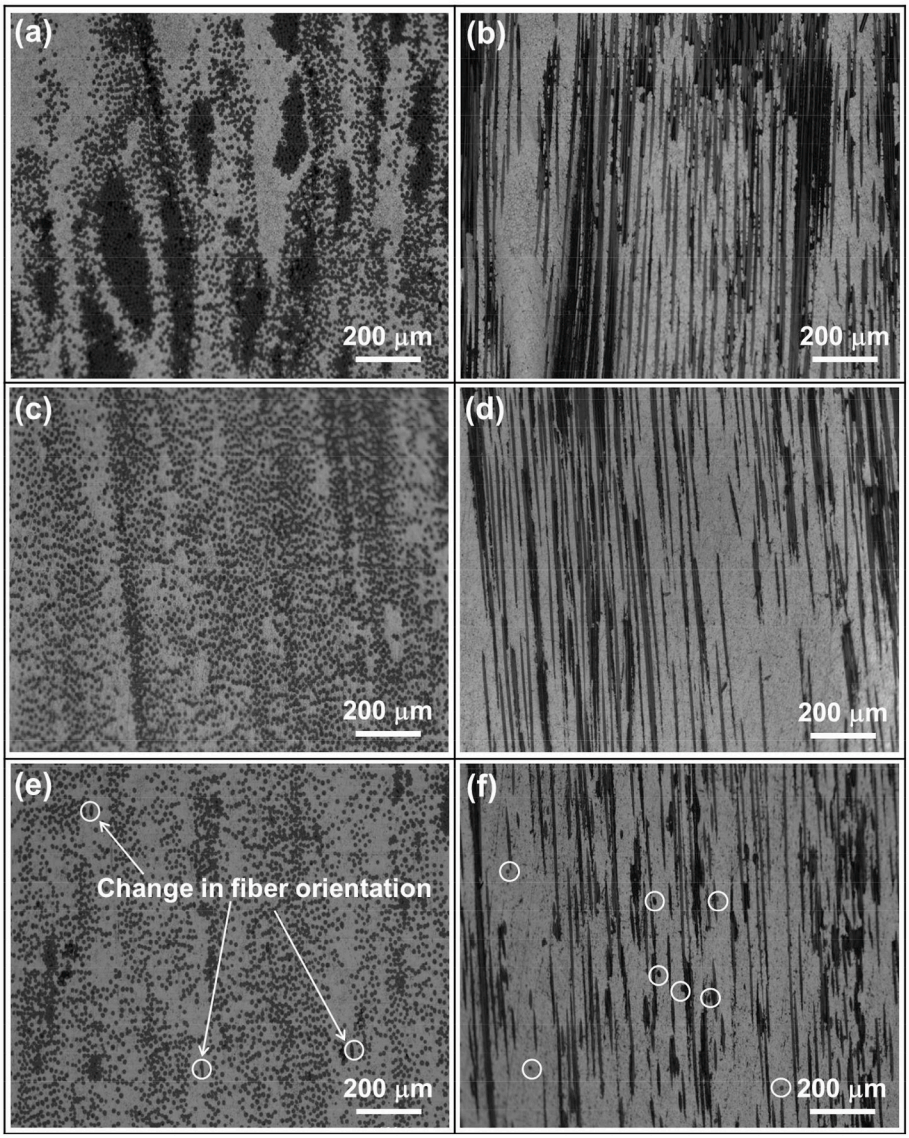

Fig. 4. Metallographic structures of 40 vol % MPCF/Al composites sintered at 650 °C/100 min under different pressures: (a) transverse, 35 MPa; (b) longitudinal, 35 MPa; (c) transverse, 45 MPa; (d) longitudinal, 45 MPa; (e) transverse, 55 MPa; (f) longitudinal, 55 MPa.

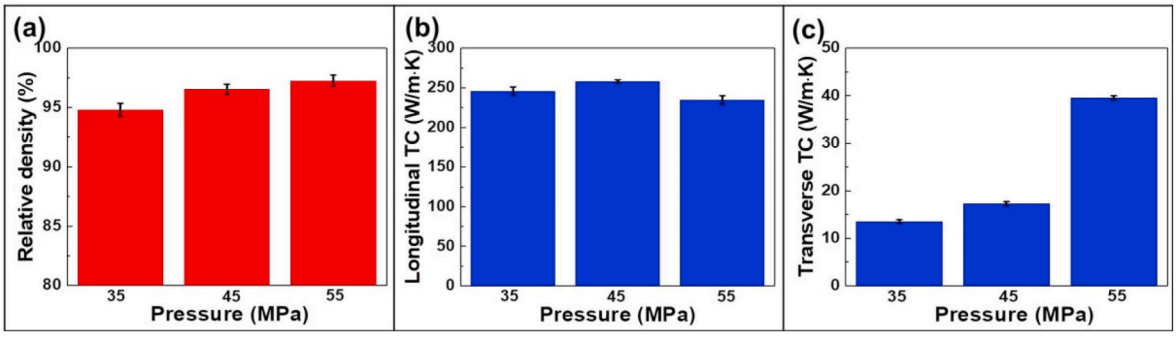

Fig. 5. Effect of sintering pressure on (a) relative density; (b) longitudinal TC; (c) transverse TC of the composites.

respectively. For the composites sintered for 40 and 60 min, no obvious diffraction peaks of Al_4C_3 can be found, but this does not mean that Al_4C_3 is not formed in the composites, because the amount of interfacial products Al_4C_3 in the composite is determined by kinetics. The reaction rate of Al_4C_3 production is determined by atomic diffusion, which can be described by the following formula: $g=(2Xt)^{1/2}$ [27,32], where g, X and t are growth amount of the Al_4C_3, growth rate constant and reaction time, respectively. Moreover, the growth rate constant is related to temperature, which can be obtained by using Arrhenius' law: $X = x\exp(-Q/RT_0)$, where x, Q, R and T_0 are the temperature constant, activation energy,

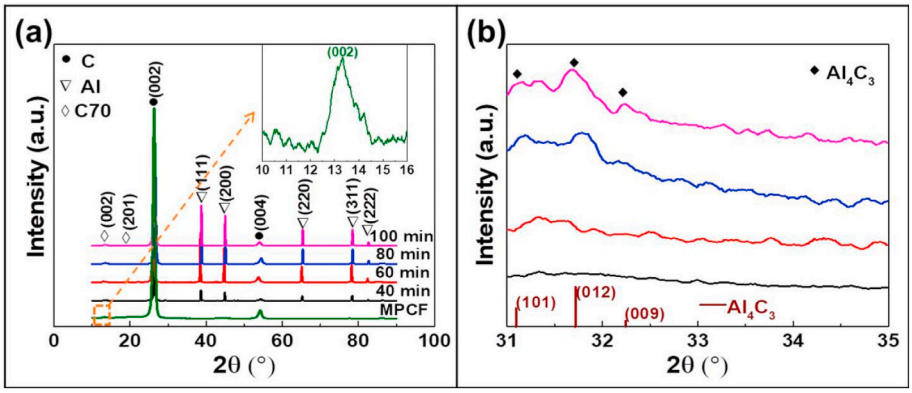

Fig. 6. XRD patterns of 40 vol % MPCF/Al composites sintered at 650 °C/45 MPa for different time: (a) 10–90° with a scan speed of 4°/min; (b) 31–35° with a scan speed of 0.25°/min.

gas constant (8.314 J/(K·mol)) and fabrication temperature, respectively [27,32]. Generally, the higher the graphitization degree of carbon fiber, the more difficult it is to react with Al to form Al_4C_3 [35]. When MPCF/Al composites are fabricated at 650 °C, *X* is a constant, which can be obtained by Ref. [27], and as the sintering time increases from 40 to 100 min, the calculated amount of Al_4C_3 in the composite will increase. Especially in the composite sintered for 80 and 100 min, the amount of Al_4C_3 is sufficient to be detected in the XRD pattern (see Fig. 6(b)).

Fig. 7 shows the relative density, longitudinal and transverse TC of the composites sintered from 40 to 100 min. As shown in Fig. 7(a), the relative density of the composites increases from 95% to 96.5% with the increase of sintering time. This is because there is more time to reduce interfacial defects and allow Al to fill up the pores left by the adjacent or intersecting fibers. As shown in Fig. 7(b) and (c), as the sintering time increases from 40 to 60 min, the longitudinal TC and transverse TC of the composites increases from 251.4 to 288.3 W/(m·K) and 13.2–17.5 W/(m·K), respectively. If the sintering time further increases to 80 and 100 min, the TC (longitudinal/transverse) of composites will decrease to 273.4/17.3 W/(m·K) and 258.1/17.3 W/(m·K), respectively. It can be explained as follows: When the composites are fabricated at a certain sintering temperature and appropriate pressure, their TC values are mainly affected by the relative density, the amount of Al_4C_3 and the local damage on MPCF surface by the interfacial reaction [27,32]. The increase of sintering time will increase the relative density and the amount of Al_4C_3, and at the same time, the local damage on MPCF surface will become more serious. The increase in relative density is conducive to the improvement of longitudinal and transverse TC of the composites, while the increase in the amount of Al_4C_3 and the serious local damage on MPCF surface will reduce the longitudinal and transverse TC of the composites. Therefore, it can be seen that when the sintering time is less than 60 min, the relative density plays a dominant role in the longitudinal and transverse TC of the composites. When the sintering time exceeds 60 min, the amount of Al_4C_3 and the local damage on MPCF surface play a leading role in the longitudinal and transverse TC of the composites. It is worth noting that when the sintering time exceeds 60 min, the longitudinal TC of the composites was significantly decreased with the increase of the sintering time, whereas the transverse TC was not affected by sintering time mostly. This can further indicate that the reduction in the longitudinal TC of the composite is mainly affected by the local damage on MPCF surface, not caused by the amount of Al_4C_3, because Al_4C_3 can give a bad effect on the TC of the composite in any direction, but in fact the transverse TC of the composite does not change much. This can also be verified in Ref. [27]. Based on the above analysis, it can be concluded that the composite possesses the highest longitudinal TC only when it is sintered for proper time (60 min in this work).

3.2. *Effect of MPCF volume fraction on microstructures and thermal-mechanical properties of MPCF/Al composites*

Pure Al and MPCF/Al composites with 20–50 vol % MPCF are fabricated by VHP under the optimized conditions, i.e. 650 °C/45 MPa/60 min. Fig. 8 shows the microstructures of MPCF/Al composites with different MPCF volume fractions. As the volume fraction increases, the MPCFs tend to be adjacent to each other. Especially when the MPCF volume fraction is 50%, a wide range of fiber agglomeration occurs in the composite as shown in Fig. 8(d), which will inevitably increase the defects in the composite.

To further understand the microstructure of the composites, TEM was used to characterize the typical interface structure. The results are shown in Fig. 9. Fig. 9(a) and (b) shows the bright and dark field images of the microstructure of the composite, respectively. It can be seen that most of the areas at the interface are “clean”, and only a small part of the area has a lath-like phase, which is likely to be the Al_4C_3 phase. The inset on the bottom left of Fig. 9(b) shows the SAD pattern of MPCF, where (002), (100), (004) and (006) diffraction rings can be identified. The

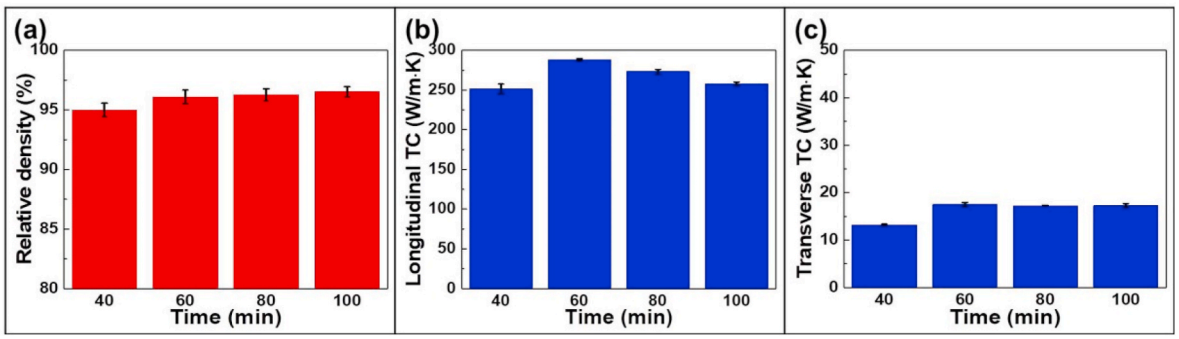

Fig. 7. Effect of sintering time on (a) relative density; (b) longitudinal TC; (c) transverse TC of the composites.

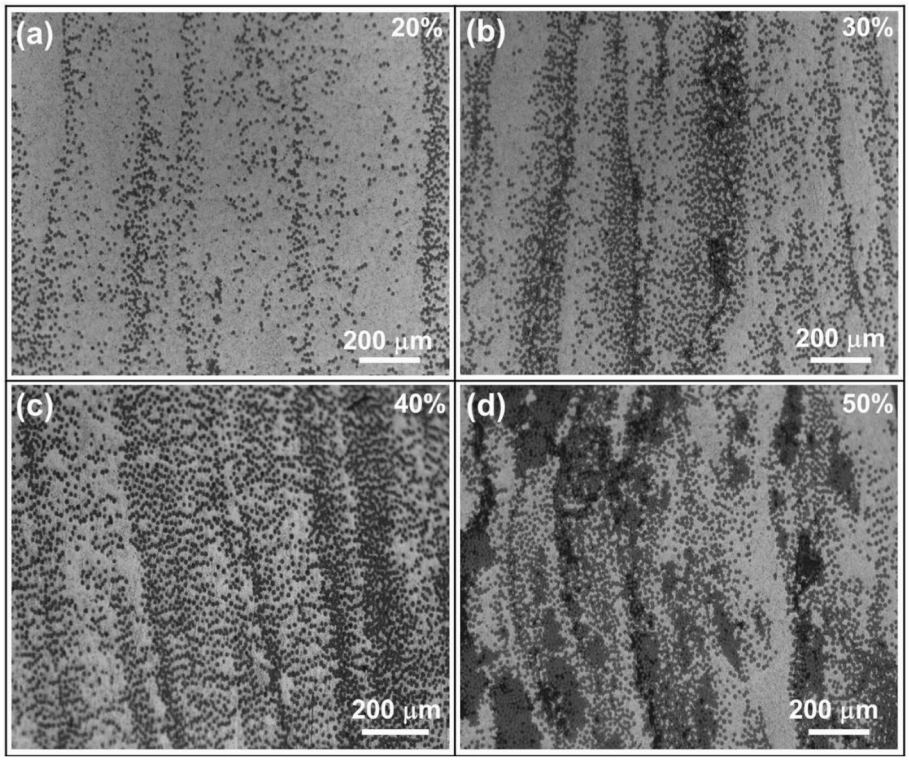

Fig. 8. Microstructures of MPCF/Al composites with different MPCF volume fraction fabricated at 650 °C/45 MPa/60 min: (a) 20 vol %; (b) 30 vol %; (c) 40 vol %; (d) 50 vol %.

inset on the top right of Fig. 9(b) shows the indexed [011] zone axis selected area diffraction (SAD) pattern of the Al. Fig. 9(c) and (d) shows the high magnification image of the interface and its EDS mapping, respectively. It can be seen that there are no obvious defects at the interface and the interface is mainly composed of O element and a small amount of C and Al elements. The O element may come from the raw carbon material or the oxide films of the Al melt during the fabrication process [36]. Fig. 9(e) shows the typical high resolution TEM (HRTEM) image of the interface and the insets are the provided Fast Fourier Transform (FFT) images of some selected areas of interface and MPCF, respectively. It can be seen that the interface layer has a thickness of approximately 2–5 nm and is tightly adhered to the Al matrix. The FFT pattern of the interface indicates that the interface layer is likely to have an amorphous structure. The interface layer with such a structure often appears in the carbon/aluminum composites and it is formed by the Al element catalyzing the surface of the carbon material, which has been confirmed in some references [36,37]. Also, it can be seen that there exist C70 phase in the MPCF, which corresponds to the XRD analysis results (see Fig. 6(a)). Fig. 9(f) shows the HRTEM image of the interface between the Al matrix and the lath-like phase. According to the Fast Fourier Transform (FFT) images of some selected areas of the Al and lath-like phase, it can be seen that the Al_4C_3 phase does exist, and its (012) plane is almost parallel to the $(11\bar{1})$ plane of Al. In short, the composites fabricated under the optimized conditions have a fine interface with good interfacial bonding and few harmful reaction products.

Table 3 summarizes the values of the thermal-physical properties of Al and MPCF/Al composites. It can be seen that the TC of Al is 220.5 W/(m·K). With the continuous addition of MPCFs, the relative density and transverse TC of the composites decreases from 98.5% to 94.2% and 50.8 to 7.5 W/(m·K), respectively, while the longitudinal TC increases from 230.3 to 288.3 W/(m·K). Therefore, the addition of MPCFs is beneficial to reduce the relative density, transverse TC and improve the longitudinal TC of the composites. However, it is worth noting that for the composite with a high MPCF volume fraction (50%), the longitudinal TC will decrease slightly due to the increase of defects.

Fig. 10(a) shows the measured and predicted longitudinal TC values of MPCF/Al composites with 20–50 vol % MPCF. The predicted longitudinal TC can be obtained by using the rule of mixture (ROM-Eq. (2)) [38]:

$$\lambda_c^L = V_f\lambda_f^L + (1 - V_f)\lambda_m \tag{2}$$

Where λ stands for the TC and superscript L refers to the longitudinal direction. The measured longitudinal TC values of these composites exceed 90% of the predictions. Moreover, the composite with 40 vol % MPCF exhibits high TC over 95% of the predictions. This is due to relatively intact and parallel MPCFs and the fine interface with good interfacial bonding and few harmful reaction products. Therefore, MPCFs can be used as effective reinforcements for Al matrix composites. Fig. 10(b) shows the measured and predicted transverse TC values of these composites. The predicted transverse TC can be obtained by the model of laminate composites (Eq. (3a), (3b) and (3c)) [32,39] and the Gurtman model (Eq. (4a) and (4b)) [40].

$$\frac{1}{\lambda_c^T} = \frac{V_f}{\lambda_f^T} + \frac{1 - V_f}{\lambda_m} + \frac{2}{d}R_e \tag{3a}$$

$$d = \frac{d_W w}{W} \tag{3b}$$

$$R_e = \frac{2\left(\rho_m\nu_m + \rho_f\nu_f\right)^2}{C_m\rho_m^2\nu_m^2\rho_f\nu_f}\left(\frac{\nu_f}{\nu_m}\right)^2 \tag{3c}$$

$$\lambda_c^T = V_f\lambda_f^T(1 + V_mA) + V_m\lambda_m\left(1 - V_fA\right) \tag{4a}$$

$$A = \frac{\lambda_m - \lambda_f^T}{\lambda_m + \lambda_f^T + V_f\left(\lambda_m + \lambda_f^T\right)} \tag{4b}$$

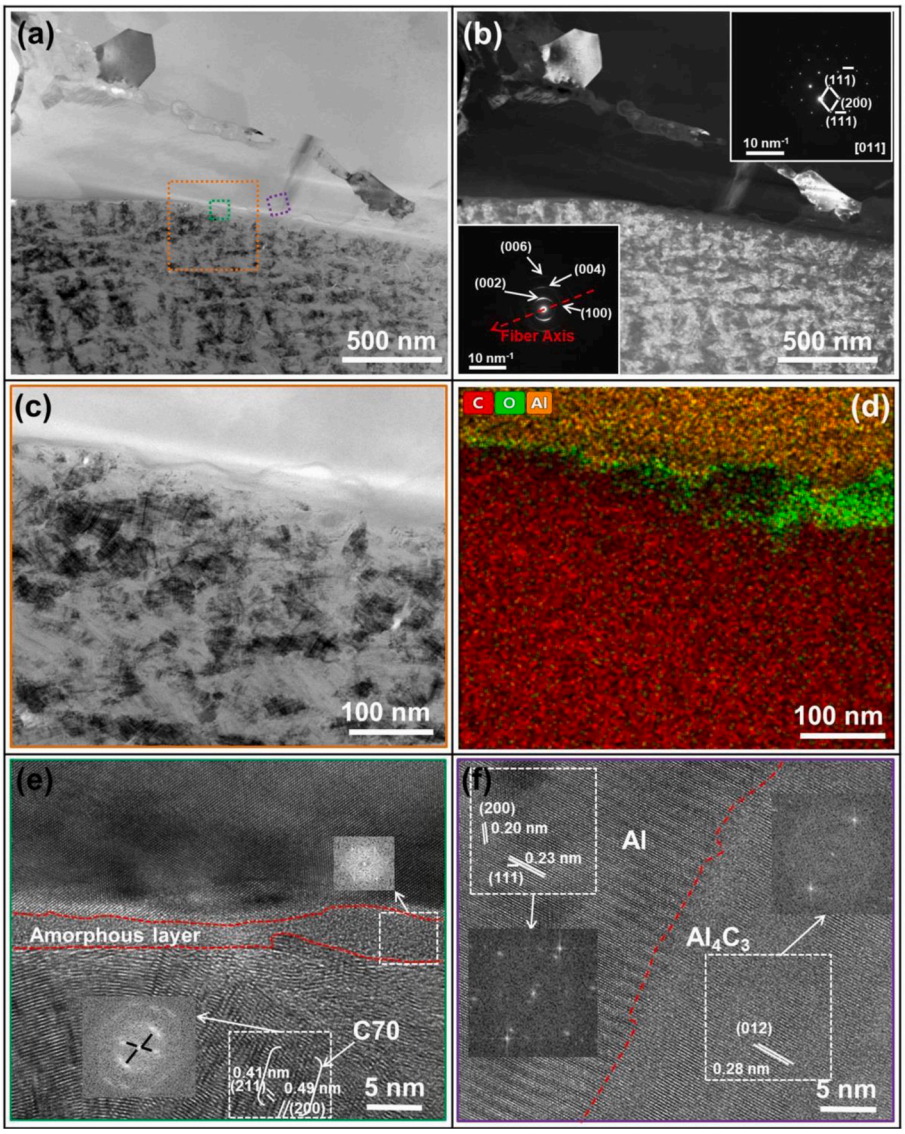

Fig. 9. Typical TEM image of the interface of the MPCF/Al composites: (a) the bright-field image; (b) the dark-field image; (c) the high magnification image of the interface; (d) EDS mapping; (e) HRTEM image of the interface; (f) HRTEM image of the interface between Al matrix and lath-like phase.

Table 3
Measured values of thermal-physical properties for Al and MPCF/Al composites with 20–50 vol % MPCF.

samples	V_f (%)	ρ (g/cm^3)	ρ_R (%)	C (J/g/K)	α (m^2/s) L T		TC (W/m·K) L T	
Al		2.69	99.7	0.880 [36]	92.7 ± 3.2		220.5 ± 7.8	
MPCF/Al	20	2.54	98.5	0.866	104.5 ± 1.7	23.1 ± 1.4	230.3 ± 3.7	50.8 ± 3.2
	30	2.45	97.1	0.863	116.4 ± 1.1	15.3 ± 1.2	246.5 ± 2.3	32.4 ± 2.5
	40	2.37	96.1	0.856	142.0 ± 0.6	8.6 ± 0.2	288.3 ± 1.3	17.5 ± 0.4
	50	2.27	94.2	0.856	143.0 ± 2.3	3.8 ± 0.1	279.3 ± 4.6	7.5 ± 0.1

Where d and w are assumed to be the thickness and mass of 0.057 g MPCFs mixed with Al powders of different weights, d_W and W stand for the thickness and mass of the composite sample, R_e is the interfacial thermal resistance of the MPCF/Al composites, ν is the phonon velocity ($\nu_m = 3620$ m/s and $\nu_f = 6792$ m/s [39]) and superscript T refers to the transverse direction. It can be seen that the measured transverse TC values of these composites locate between the two models, and as MPCF volume fraction increases, they are close to the model of laminate composites. There may be two main reasons for this phenomenon. One is that the longitudinal TC of the composites is much higher than the transverse TC. When testing the transverse TC of the composites, heat is more likely to be conducted in the longitudinal direction and then dissipated, which will result in relatively lower TC along the transverse direction. The other is that as the MPCF volume fraction increases, MPCFs tend to be adjacent to each other. When the heat is conducted in the transverse direction, the heat conduction path will inevitably become longer where the MPCFs gather, thereby reducing the efficiency of heat conduction. These can be seen from the schematic diagrams of longitudinal and transverse heat conduction paths as shown in Fig. 10 (c).

Fig. 11 shows the longitudinal and transverse thermal expansion

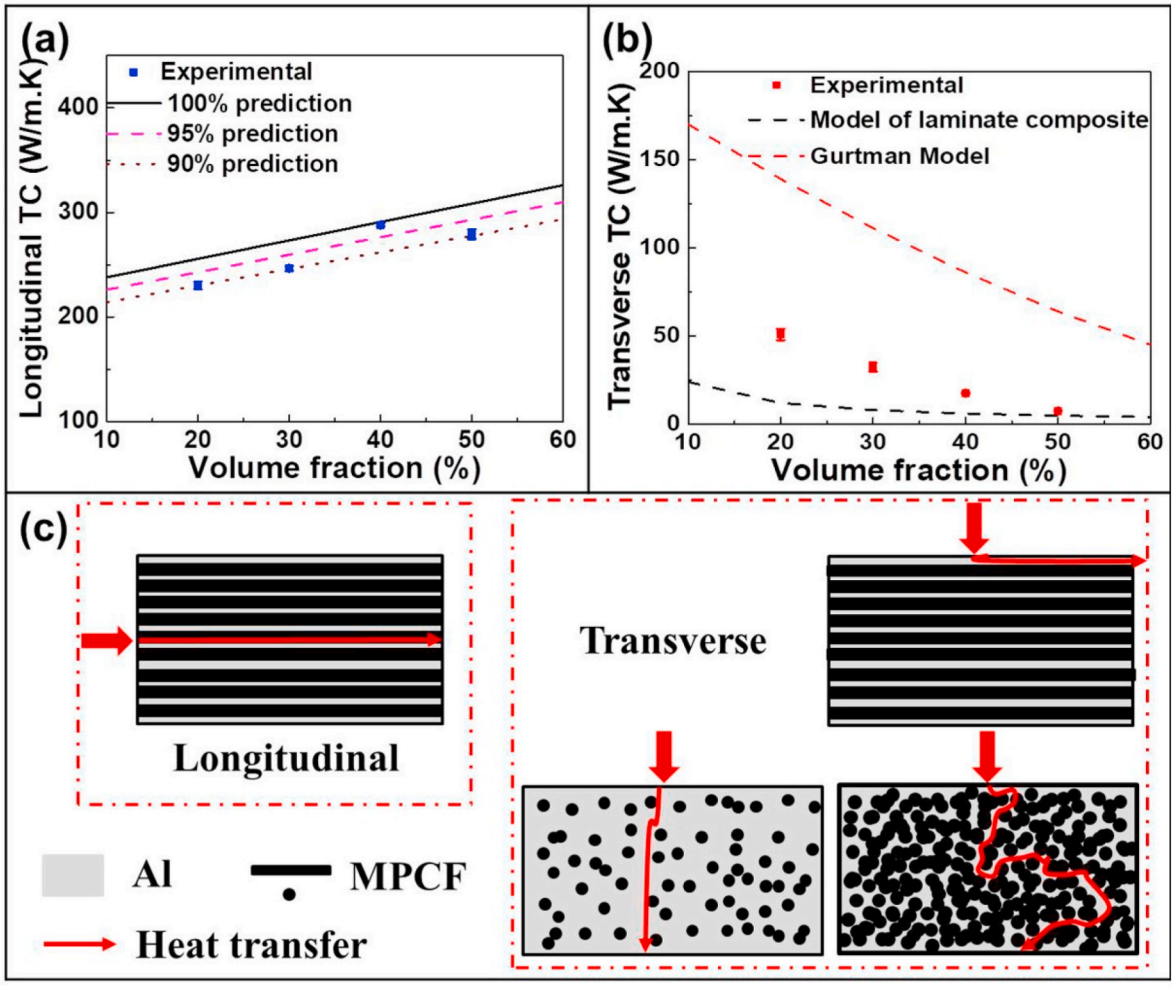

Fig. 10. Comparison of (a) measured values of longitudinal TC with the rule of mixture; (b) measured values of transverse TC with the model of laminate composite and Gurtman model; (c) Schematic diagrams of longitudinal and transverse heat conduction path.

curve and average CTE of the composites before and after thermal cycling (0, 50 and 100 cycles). For comparison, the thermal expansion curve and average CTE of pure Al are also measured. As shown in Fig. 11 (a), the length change of the composites without thermal cycling in the longitudinal direction shows a decreasing trend with the increase of the MPCF volume fraction. At the same time, it can be noticed that there is an unsteady state in the thermal expansion curve during the initial heating stage, which is caused by the internal stress [41]. After that, the slope of thermal expansion curve tends to be stable. On the whole, the length change is not great, and the length of 20 vol % MPCF/Al composite has only increased by 0.044%, because MPCF has a negative CTE in the longitudinal direction, and gradually shrinks as the temperature increases, thereby inhibiting the plastic deformation of Al. After 50 and 100 thermal cycles, the thermal expansion curve of the composites changes little compared with that without thermal cycling, which is due to the fine interface obtained by using an optimized fabrication process. As shown in Fig. 11(b), the length change of the composites and pure Al without thermal cycling in the transverse direction shows an increasing trend with the increase of the temperature, because both MPCF and Al expand in the transverse direction during the heating process. Similarly, the thermal expansion curve of the composites does not change much after 50 and 100 thermal cycles. As shown in Fig. 11(c) and (d), in the temperature range of 25–250 °C, with the increase of the MPCF volume fraction, the longitudinal CTE of the composites without thermal cycling decreases from 2.28 to −0.22 ppm/K and transverse CTE varies from 31.4 to 26.8 ppm/K, while the average CTE of Al is 24.6 ppm/K, indicating that the addition of MPCFs is beneficial to reduce the longitudinal CTE of the composite. Among them, the longitudinal CTE values of the composites with 40 and 50 vol % MPCF are near zero expansion. After 50 and 100 thermal cycles, it can be seen that the thermal cycle has little effect on the longitudinal and transverse CTE of those composites, and the composites with 40 and 50 vol % MPCF are more likely to provide good dimensional stability in the longitudinal direction.

Fig. 12 shows the mechanical properties and fracture surfaces of pure Al and the composites. As shown in Fig. 12(a), the dimension and shape of the tensile specimens can be specifically understood, and according to the longitudinal tensile stress-strain curves of pure Al and the composites, it can be seen that the composites exhibit higher elastic modulus, tensile strength, and lower elongation than the matrix. As shown in Fig. 12(b), the elastic modulus and tensile strength of pure Al is 70.5 GPa and 103 MPa, respectively. As the MPCF volume fraction increases, the elastic modulus of the composites increases from 147.5 to 324 GPa, while the tensile strength shows a trend of increasing first and then decreasing. When the MPCF volume fraction is 40%, the tensile strength reaches the maximum, which is 177.2 MPa. Compared with the Al matrix, the elastic modulus and tensile strength of the composites are increased by 359.6% and 72% at the highest. As shown in Fig. 12(c), the fracture surface of 40 vol % MPCF/Al composite is uneven and some fibers are pulled out of the matrix, indicating that the interfacial reaction between the MPCF and the matrix is not very serious. Only partially debondings take place during loading so loads transfer can still go on which lead to the improvement of the tensile properties of the

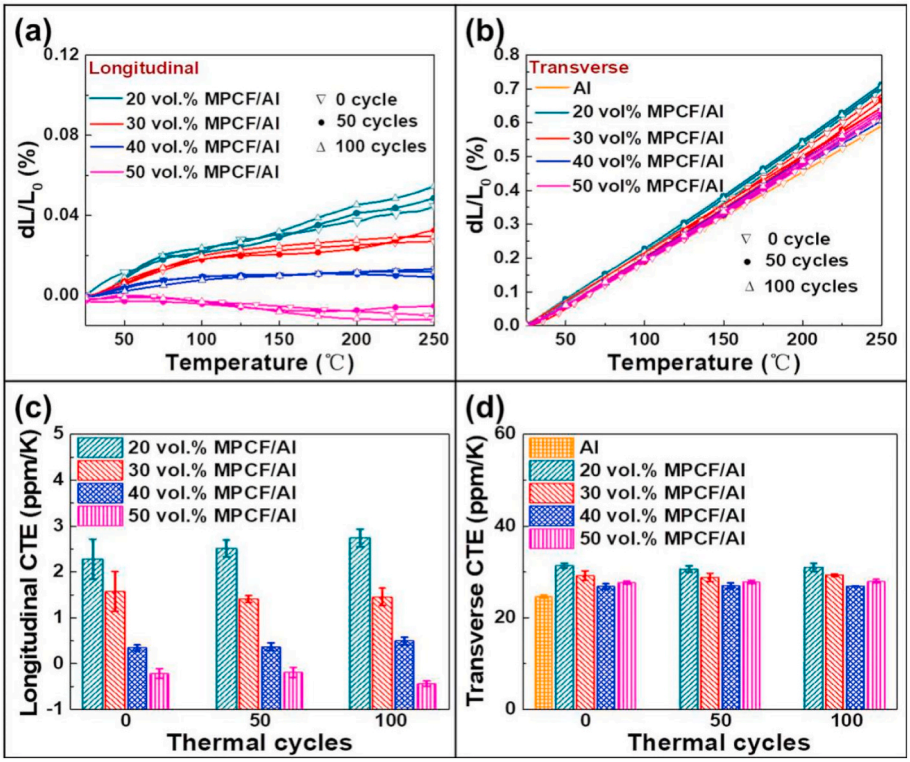

Fig. 11. Effect of MPCF volume fraction and thermal cycles on (a) longitudinal thermal expansion curve; (b) transverse thermal expansion curve; (c) longitudinal CTE; (d) transverse CTE of the composites.

composite. As shown in Fig. 12(d), although some fibers are pulled out of the matrix on the fracture surface of 50 vol % MPCF/Al composite, there are obvious cracks in the fracture at the same time, which is caused by fiber agglomeration, so the tensile strength of the composite is decreased.

3.3. Comparisons with other kinds of Al matrix composites and Al alloys

Fig. 13(a) shows the TC with respect to CTE of Al matrix composites with 20–50 vol % reinforcement (including SiC [42], diamond [43,44], AlN [45,46], GF [33], Gr film [36,47] and MPCF [10,48]) and Al alloys [49] that may be used as thermal management materials. It can be seen that the TC values of MPCF/Al composites in this work are at a medium level, but the CTE values are lower than those of Al matrix composites and Al alloy in the references. Fig. 13(b) shows the elastic modulus with respect to density of Al matrix composites with 20–50 vol % reinforcement [50–52] and Al alloys [49]. It can be seen that the MPCF/Al composites in this work have a high specific modulus (elastic modulus per unit density). The main reasons why these composites have good TC, low CTE and high specific modulus are as follows: (1) MPCF has the longitudinal TC of 396.4 W/m·K, negative CTE of −1.5 ppm/K, density of 2.12 g/cm^3 and elastic modulus of 750 GPa, which is expected to be a reinforcement for unidirectional thermal management materials with integrated structure and function. (2) For continuous MPCF/Al composites, it is relatively easy to control the orientation of the MPCFs by controlling the mixing of MPCFs and Al powders. Therefore, it is easier to bring the enhancement effect of the MPCFs into full play. (3) Although graphite also has a negative CTE, the CTE of MPCF/Al composites is lower than that of graphite/Al composites, because the size of the fiber is smaller, the interfaces in the MPCF/Al composites are more, and the impact on the CTE of the composites is greater. (4) MPCF/Al composites fabricated in this work have a fine interface as shown in Fig. 9. Perhaps the TC of this composite can be further improved by using MPCFs with higher TC as the reinforcement.

4. Conclusions

To meet the requirements of thermal management materials with good TC, low CTE and resistance to deformation, continuous MPCF/Al composites were fabricated by VHP in this work. The effect of process parameters on the microstructures and TC of MPCF/Al composites was studied. Furthermore, the influence of MPCF volume fraction on the microstructures, interfaces and thermal-mechanical properties of the composites under optimized process conditions was investigated, and their thermal-mechanical properties were compared with those of other kinds of Al matrix composites and Al alloys. Main conclusions can be summarized as:

(1) 40 vol % MPCF/Al composites with high longitudinal TC were successfully fabricated under the process conditions of 650 °C/45 MPa/60 min, and high longitudinal TC resulted from the following microstructural characteristics: (a) suitable interfacial bonding, (b) relatively intact and parallel MPCFs, (c) controllable interfacial reaction.

(2) The interface between MPCF and Al is mainly composed of an amorphous interface layer of 2–5 nm, which mainly contains O elements and a small amount of Al and C elements. At the same time, there is a very small amount of lath-like carbide crystal at the interface, its (012) plane is almost parallel to the $(11\bar{1})$ plane of the matrix.

(3) The longitudinal TC of the composites with 20–50 vol % MPCF is 230.3–288.3 W/(m·K), which exceeds 90% of the predictions by the rule of mixture. The transverse TC is 50.8–7.5 W/(m·K), which tends to be the predicted value by the model of laminate composites with the increase of MPCF volume fraction. The longitudinal and transverse CTE values are 2.28−-0.22 ppm/K and 31.4–26.8 ppm/K, respectively. After 50 and 100 thermal cycles, their CTE values do not change much. Compared with the Al

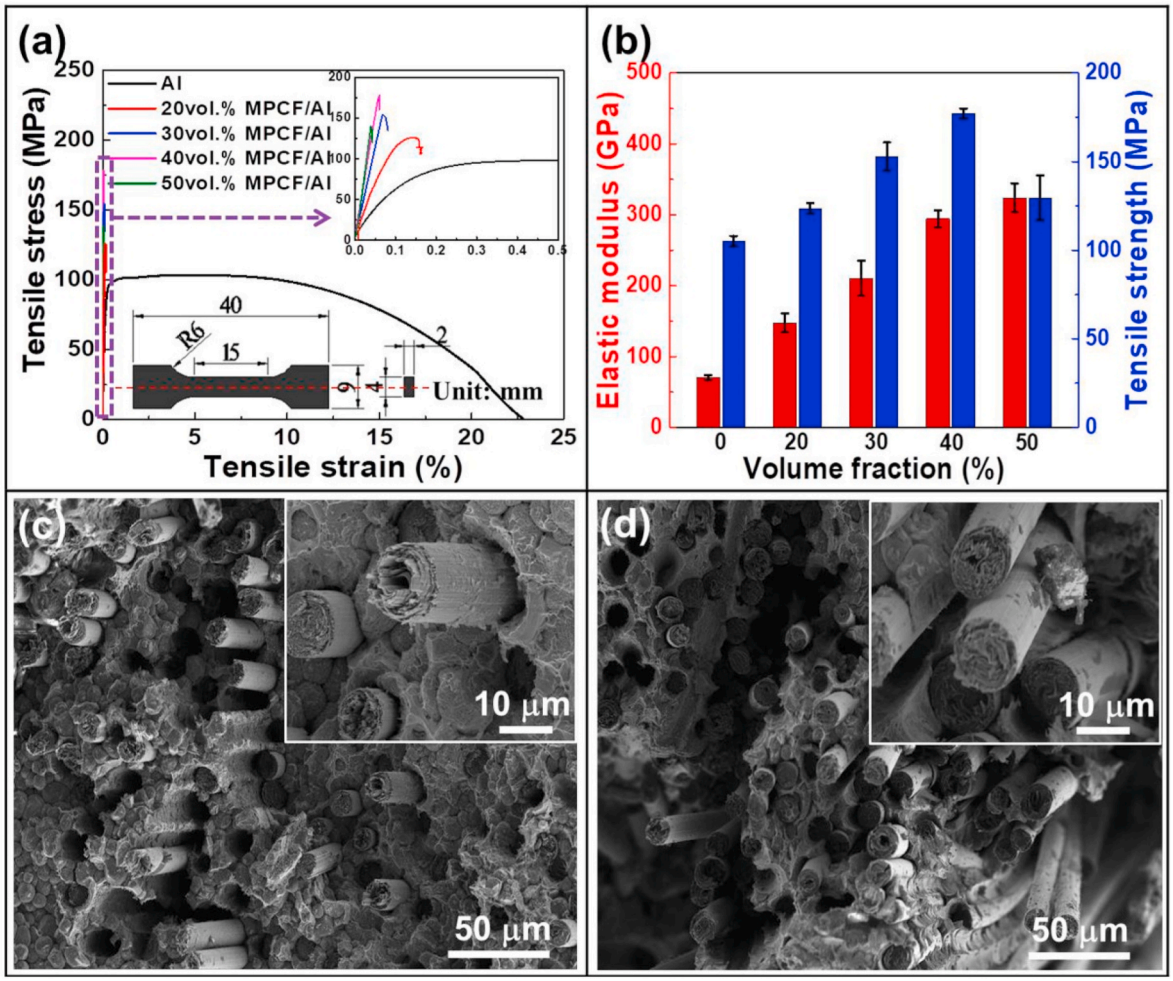

Fig. 12. Mechanical properties of Al and MPCF/Al composites with 20–50 vol % MPCF: (a) tensile stress-strain curves, (b) comparative study of the elastic modulus and tensile strength; Fracture surfaces of (c) 40 vol % MPCF/Al composite, (d) 50 vol % MPCF/Al composite.

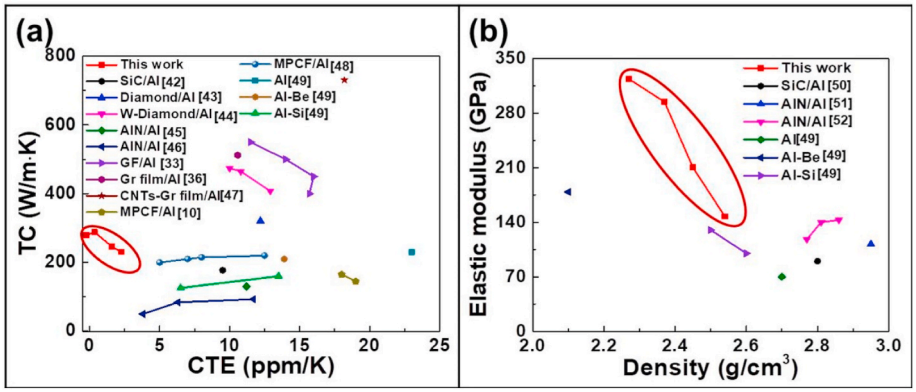

Fig. 13. (a) The TC versus CTE; (b) The elastic modulus versus density of Al matrix composites with 20–50 vol % reinforcement and Al alloy selected as thermal management materials.

matrix, the elastic modulus and tensile strength of the composites are increased by 359.6% and 72% at the highest.

(4) Compared with other Al matrix composites and Al alloys that may be used as thermal management materials, the TC values of MPCF/Al composites in this work are at a medium level, but their CTE values and specific modulus are more advantageous, and their TC values may be further improved by using MPCFs with higher TC, so these composites are expected to become unidirectional thermal management materials with integrated structure and function.

Author statement

Chengnan Zhu: Methodology, Investigation, Data curation, Formal analysis, Writing -original draft.

Yishi Su: Conceptualization, Validation, Writing - review & editing,

Supervision.

Xiaoshu Wang: Data curation, Formal analysis.

Haicheng Sun: Resources.

Di Zhang: Project administration, Validation.

Qiubao Ouyang: Conceptualization, Resources, Funding acquisition, Supervision.

Declaration of competing interest

The authors declare that they have no known competing financial interests or personal relationships that could have appeared to influence the work reported in this paper.

Acknowledgments

This work was supported by the National Key Research and Development Progress of China (Nos. 2018YFB0704400, 2017YFB0406100) and the National Natural Science Foundation of China (Nos. 51671129, 51971132, 51501111, 51471106).

References

[1] Cho HJ, Kim Y-J, Erb U. Thermal conductivity of copper-diamond composite materials produced by electrodeposition and the effect of TiC coatings on diamond particles. Compos B Eng 2018;155:197–203.
[2] Xu T, Zhou S, Cui S, Song N, Shi L, Ding P. Three-dimensional carbon fiber-graphene network for improved thermal conductive properties of polyamide-imide composites. Compos B Eng 2019;178:107495.
[3] Jang J-H, Park H-K, Lee J-H, Lim J-W, Oh I-H. Effect of volume fraction and unidirectional orientation controlled graphite on thermal properties of graphite/copper composites. Compos B Eng 2020;183:107735.
[4] Mizuuchi K, Inoue K, Agari Y, Nagaoka T, Sugioka M, Tanaka M, et al. Processing of Al/SiC composites in continuous solid–liquid co-existent state by SPS and their thermal properties. Compos B Eng 2012;43(4):2012–9.
[5] Nazeer F, Ma Z, Gao L, Wang F, Khan MA, Malik A. Thermal and mechanical properties of copper-graphite and copper-reduced graphene oxide composites. Compos B Eng 2019;163:77–85.
[6] Huang Y, Ouyang Q, Zhang D, Zhu J, Li R, Yu H. Carbon materials reinforced aluminum composites: a review. Acta Metall Sin 2014;27(5):775–86.
[7] Kurita H, Miyazaki T, Kawasaki A, Lu Y, Silvain J-F. Interfacial microstructure of graphite flake reinforced aluminum matrix composites fabricated via hot pressing. Compos Appl Sci Manuf 2015;73:125–31.
[8] Qu X-h, Zhang L, Wu M, Ren S-b. Review of metal matrix composites with high thermal conductivity for thermal management applications. Prog Nat Sci Mater Int 2011;21(3):189–97.
[9] Lalet G, Kurita H, Heintz J-M, Lacombe G, Kawasaki A, Silvain J-F. Thermal expansion coefficient and thermal fatigue of discontinuous carbon fiber-reinforced copper and aluminum matrix composites without interfacial chemical bond. J Mater Sci 2013;49(1):397–402.
[10] Veillere A, Kurita H, Kawasaki A, Lu Y, Heintz JM, Silvain JF. Aluminum/carbon composites materials fabricated by the powder metallurgy process. Materials 2019;12(24).
[11] Zhou W, Mikulova P, Fan Y, Kikuchi K, Nomura N, Kawasaki A. Interfacial reaction induced efficient load transfer in few-layer graphene reinforced Al matrix composites for high-performance conductor. Compos B Eng 2019;167:93–9.
[12] Şenel MC, Gürbüz M, Koç E. Fabrication and characterization of synergistic Al-SiC-GNPs hybrid composites. Compos B Eng 2018;154:1–9.
[13] Zhu C, Su Y, Zhang D, Ouyang Q. Effect of Al2O3 coating thickness on microstructural characterization and mechanical properties of continuous carbon fiber reinforced aluminum matrix composites. Mater Sci Eng A 2020;793:139839.
[14] Xu Z, Li D, Wang P, Jiang L, Chen G, Wu G. Effect of TM (TM=Fe, Mn, Cr) alloying on the high temperature properties and strengthening mechanism of Cf/Al composites. Compos B Eng 2021:108622.
[15] Newcomb BA. Processing, structure, and properties of carbon fibers. Compos Appl Sci Manuf 2016;91:262–82.
[16] Kim K-W, Jeong J-S, An K-H, Kim B-J. A study on the microstructural changes and mechanical behaviors of carbon fibers induced by optimized electrochemical etching. Compos B Eng 2019;165:764–71.
[17] Shirasu K, Goto K, Naito K. Microstructure-elastic property relationships in carbon fibers: a nanoindentation study. Compos B Eng 2020;200:108342.
[18] Liu Q, He X-B, Ren S-B, Liu T-T, Kang Q-P, Qu X-H. Fabrication and thermal conductivity of copper matrix composites reinforced with Mo2C or TiC coated graphite fibers. Mater Res Bull 2013;48(11):4811–7.
[19] Shirvanimoghaddam K, Hamim SU, Karbalaei Akbari M, Fakhrhoseini SM, Khayyam H, Pakseresht AH, et al. Carbon fiber reinforced metal matrix composites: fabrication processes and properties. Compos Appl Sci Manuf 2017;92:70–96.
[20] Cao X, Shi Q, Liu D, Feng Z, Liu Q, Chen G. Fabrication of in situ carbon fiber/aluminum composites via friction stir processing: evaluation of microstructural, mechanical and tribological behaviors. Compos B Eng 2018;139:97–105.
[21] Wang Z, Yang S, Du Z, Jiang W, Zhang A, Cai C, et al. Micromechanical modeling of damage evolution and mechanical behaviors of CF/Al composites under transverse and longitudinal tensile loadings. Materials 2019;12(19).
[22] Wang Z, Wang Z, Xiong B, Cai C, Xu Z, Yu H. Micromechanics analysis on the microscopic damage mechanism and mechanical behavior of graphite fiber-reinforced aluminum composites under transverse tension loading. J Alloys Compd 2020;815:152459.
[23] Wang Z, Wang Z, Liu Y, Cai C, Xiong B, Wang Z, et al. Simulation and experimental study of mechanical and fracture behavior of 2.5D woven C-fiber/aluminum composites under warp directional tension loading. Fatig Fract Eng Mater Struct 2021;44(2):383–96.
[24] Idinsk K, Simank F, Korb Ac J, Kramer I, Zemnkov M, tefnik P, et al. Preparation and thermophysical properties of Cu alloy-high thermal conductivity carbon fibre composites. Kovove Mater 2006;44(6):327–34.
[25] Zhang Y-h, Wu G-h. Interface and thermal expansion of carbon fiber reinforced aluminum matrix composites. Trans Nonferrous Metals Soc China 2010;20(11):2148–51.
[26] Rawal SP. Metal-matrix composites for space applications. JOM 2001;53:14–7.
[27] Lee M, Choi Y, Sugio K, Matsugi K, Sasaki G. Effect of aluminum carbide on thermal conductivity of the unidirectional CF/Al composites fabricated by low pressure infiltration process. Compos Sci Technol 2014;97:1–5.
[28] Choi Y, Gen S, Kazuhiro M, Kenjiro S, Lee M. Influence of Si addition on thermal conductivity of unidirectional CF/Al-Si composites fabricated by low pressure infiltration process. Mater Res Innovat 2015;19(sup9). S9-162-S9-6.
[29] Pei R, Chen G, Wang Y, Zhao M, Wu G. Effect of interfacial microstructure on the thermal-mechanical properties of mesophase pitch-based carbon fiber reinforced aluminum composites. J Alloys Compd 2018;756:8–18.
[30] Sree Manu KM, Ajay Raag L, Rajan TPD, Pai BC, Petley V, Verma SN. Self-lubricating bidirectional carbon fiber reinforced smart aluminum composites by squeeze infiltration process. J Mater Sci Technol 2019;35(11):2559–69.
[31] Tan Z, Li Z, Fan G, Kai X, Ji G, Zhang L, et al. Diamond/aluminum composites processed by vacuum hot pressing: microstructure characteristics and thermal properties. Diam Relat Mater 2013;31:1–5.
[32] Huang Y, Su Y, Li S, Ouyang Q, Zhang G, Zhang L, et al. Fabrication of graphite film/aluminum composites by vacuum hot pressing: process optimization and thermal conductivity. Compos B Eng 2016;107:43–50.
[33] Chen JK, Huang IS. Thermal properties of aluminum–graphite composites by powder metallurgy. Compos B Eng 2013;44(1):698–703.
[34] Liu T, He X, Liu Q, Ren S, Zhang L, Qu X. Preparation and thermal conductivity of spark plasma sintered aluminum matrix composites reinforced with titanium-coated graphite fibers. Adv Eng Mater 2015;17(4):502–11.
[35] Seong HG, Lopez HF, Robertson DP, Rohatgi PK. Interface structure in carbon and graphite fiber reinforced 2014 aluminum alloy processed with active fiber cooling. Mater. Sci. Eng. A 2008;487(1–2):201–9.
[36] Huang Y, Ouyang Q, Guo Q, Guo X, Zhang G, Zhang D. Graphite film/aluminum laminate composites with ultrahigh thermal conductivity for thermal management applications. Mater Des 2016;90:508–15.
[37] Khalid FA, Beffort O, Klotz UE, Keller BA, Gasser P. Microstructure and interfacial characteristics of aluminium–diamond composite materials. Diam Relat Mater 2004;13(3):393–400.
[38] Hassanzadeh-Aghdam MK, Mahmoodi MJ, Jamali J, Ansari R. A new micromechanical method for the analysis of thermal conductivities of unidirectional fiber/CNT-reinforced polymer hybrid nanocomposites. Compos B Eng 2019;175:107137.
[39] Liu T, He X, Liu Q, Ren S, Kang Q, Zhang L, et al. Effect of chromium carbide coating on thermal properties of short graphite fiber/Al composites. J Mater Sci 2014;49(19):6705–15.
[40] Koráb J, Štefánik P, Kavecký Š, Šebo P, Korb G. Thermal conductivity of unidirectional copper matrix carbon fibre composites. Compos Appl Sci Manuf 2002;33(4):577–81.
[41] Tao Z, Guo Q, Gao X, Liu L. Graphite fiber/copper composites with near-zero thermal expansion. Mater Des 2012;33:372–5.
[42] Lee HS, Jeon KY, Kim HY, Hong SH. Fabrication process and thermal properties of SiCp/Al metal matrix composites for electronic packaging applications. J Mater Sci 2000;35:6231–6.
[43] Long J, Li X, Fang D, Peng P, He Q. Fabrication of diamond particles reinforced Al-matrix composites by hot-press sintering. Int J Refract Met Hard Mater 2013;41:85–9.
[44] Zhang C, Cai Z, Wang R, Peng C, Qiu K, Wang N. Microstructure and thermal properties of Al/W-coated diamond composites prepared by powder metallurgy. Mater Des 2016;95:39–47.
[45] Zhang Q, Chen G, Wu G, Xiu Z, Luan B. Property characteristics of a AlNp/Al composite fabricated by squeeze casting technology. Mater Lett 2003;57:1453–8.
[46] Liu YQ, Cong HT, Cheng HM. Thermal properties of nanocrystalline Al composites reinforced by AlN nanoparticles. J Mater Res 2011;24(1):24–31.
[47] Chang J, Zhang Q, Lin Y, Zhou C, Yang W, Yan L, et al. Carbon nanotubes grown on graphite films as effective interface enhancement for an aluminum matrix laminated composite in thermal management applications. ACS Appl Mater Interfaces 2018;10(44):38350–8.
[48] Chamroune N, Delange F, Caillault N, Morvan F, Lu Y, Kawasaki A, et al. Synergetic effect of discontinuous carbon fibers and graphite flakes on thermo-mechanical properties of aluminum matrix composites fabricated by solid–liquid phase sintering. Met Mater Int 2019;26(2):155–67.
[49] Zweben C. Advances in composite materials for thermal management in electronic packaging. JOM 1998;50:47–51.

[50] Inoue A, Nosaki K, Kim BG, Yamaguchi T, Masumoto T. Mechanical strength of ultra-fine AI-AIN composites produced by a combined method of plasma-alloy reaction, spray deposition and hot pressing. J Mater Sci 1993;28:4398–404.
[51] Qu S, Geng L, Han J. SiCp-Al composites fabricated by modified squeeze casting technique. J Mater Sci Technol 2007;23:641–4.
[52] Liu YQ, Cong HT, Wang W, Sun CH, Cheng HM. AlN nanoparticle-reinforced nanocrystalline Al matrix composites: fabrication and mechanical properties. Mater. Sci. Eng. A 2009;505(1–2):151–6.
[53] Liu T, He X, Liu Q, Zhang L, Wang L, Kang Q, et al. Fabrication of short graphite fiber preforms for liquid metal infiltration. J Mater Eng Perform 2012;22(6):1649–54.
[54] Liu T, He X, Zhang L, Liu Q, Qu X. Fabrication and thermal conductivity of short graphite fiber/Al composites by vacuum pressure infiltration. J Compos Mater 2013;48(18):2207–14.
[55] Tokunaga T, Takahashi K, Ohno M, Sasaki K, Imanishi T, Matsuura K. Fabrication of carbon fiber oriented Al–based composites by hot extrusion and evaluation of their thermal conductivity. Mater Trans 2017;58(6):938–44.
[56] Choi Y, Kataoka Y, Zu Z, Matsugi K, Sasaki G. Manufacturing process of carbon-alumina short fiber hybrid reinforced aluminum matrix composites by low pressure casting. Mater Trans 2017;58(7):1097–9.
[57] Meng X, Choi Y, Matsugi K, Xu Z, Liu W. Microstructures of carbon fiber and hybrid carbon fiber-carbon nanofiber reinforced aluminum matrix composites by low pressure infiltration process and their properties. Mater Trans 2018;59(12):1935–42.
[58] Miranda AT, Bolzoni L, Barekar N, Huang Y, Shin J, Ko S-H, et al. Processing, structure and thermal conductivity correlation in carbon fibre reinforced aluminium metal matrix composites. Mater Des 2018;156:329–39.
[59] Kurita H, Feuillet E, Guillemet T, Heintz J-M, Kawasaki A, Silvain J-F. Simple fabrication and characterization of discontinuous carbon fiber reinforced aluminum matrix composite for lightweight heat sink applications. Acta Metall Sin 2014;27(4):714–22.